Nano Research
DOI 10.1007/s12274-014-0592-y
Research Article
ISSN 1998-0124
CN 11-5974/O4

Efficient $CH_3NH_3PbI_3$ perovskite solar cells with 2TPA-*n*-DP hole-transporting layers

Lifeng Zhu[1], Junyan Xiao[1], Jiangjian Shi[1], Junjie Wang[2], Songtao Lv[1], Yuzhuan Xu[1], Yanhong Luo[1], Yin Xiao[2], Shirong Wang[2], Qingbo Meng[1] (✉), Xianggao Li[2] (✉), and Dongmei Li[1] (✉)

[1] *Key Laboratory for Renewable Energy (CAS), Beijing Key Laboratory for New Energy Materials and Devices, Beijing National Laboratory for Condense Matter Physics, Institute of Physics, Chinese Academy of Sciences, Beijing 100190, China*
[2] *Collaborative Innovation Center of Chemical Science and Engineering (Tianjin), School of Chemical Engineering and Technology, Tianjin University, Tianjin 300072, China*

Received: 30 June 2014
Revised: 16 September 2014
Accepted: 19 September 2014

KEYWORDS
perovskite solar cells,
organolead halide,
hole-transporting materials,
interfacial recombination

ABSTRACT

$CH_3NH_3PbI_3$ perovskite solar cells with 2TPA-*n*-DP (TPA = 4,4′-((1E, 1′E,3E,3′E)-[1,1′-biphenyl]-4,4′-diylbis(buta-1,3-diene-4,1-diyl)); DP = bis(*N*,*N*-di-p-tolylaniline); *n* = 1, 2, 3, 4) as hole-transporting materials (HTMs) have been fabricated. After optimization of the mesoporous TiO_2 film thickness, devices based on 2TPA-2-DP with power conversion efficiencies (PCEs) of up to 12.96% have been achieved, comparable to those of devices with (2,2′,7,7′-tetrakis(*N*,*N*-di-p-methoxyphenylamine)-9,9′-spirobifluorene) (spiro-OMeTAD) as HTM under similar conditions. Further time-resolved photoluminescence (PL) measurements showed a fast charge transfer process at the perovskite/2TPA-2-DP interface. With the aid of electrochemical impedance spectra, a study of the electron blocking ability of 2TPA-2-DP in the device reveals that the presence of 2TPA-2-DP can greatly increase charge transfer resistance at the HTM/Au interface in the device, thus reducing the recombination. Furthermore, the perovskite solar cells based on these four HTMs exhibit good stability after testing for one month.

1 Introduction

Inorganic–organic hybrid perovskites are a kind of semiconductors with ABX_3 structure consisting of metal cations (B = Pb, Sn) in six-fold coordination surrounded by an octahedron of halide anions (X = Cl^-, Br^-, I^-) together with protonated organic amines (A = $CH_3NH_3^+$, $NH_2CH{=}NH_2^+$) in 12-fold cuboctahedral coordination [1, 2]. It has been shown that such layered perovskite materials can exhibit excellent characteristics, such as a suitable direct bandgap, high absorption coefficients, satisfactory carrier transportation properties and good tolerance of defects, which make them attractive photovoltaic materials [3–5]. Typically, their low cost and easy fabrication can meet basic commercialization requirements. Recently, a new type

Address correspondence to Qingbo Meng, qbmeng@iphy.ac.cn; Xianggao Li, lixianggao@tju.edu.cn; Dongmei Li, dmli@iphy.ac.cn

of photovoltaic technology based on organolead halide perovskites has developed rapidly and attracted great attention around the world [6–8]. In 2009, Miyasaka et al. first used organolead halides $CH_3NH_3PbX_3$ (X = Br^-, I^-) as light absorbers for liquid-junction sensitized solar cells and gained a power conversion efficiency (PCE) of 3.81% [9]. However, the dissolution of $CH_3NH_3PbI_3$ in liquid electrolytes resulted in serious instability of the device [10]. This problem can be well solved by replacing liquid electrolytes with solid-state hole conductors, such as 2,2′,7,7′-tetrakis(*N*,*N*-di-p-methoxyphenylamine)-9,9′-spirobifluorene (spiro-OMeTAD) [11]. Since then, unexpected breakthroughs and a rapid increase in PCEs of perovskite solar cells have been regularly reported [12–15]. To date, PCEs as high as 17.9% have been reported for single-junction perovskite solar cells, exceeding the values for sensitized solar cells and organic photovoltaics [16]. PCEs of over 20% have been predicted, suggesting this technology may be a strong competitor to commercial thin film solar cells (based on e.g. CdTe and copper indium gallium selenide (CIGS)) [17].

$CH_3NH_3PbI_3$-based solar cells are usually composed of fluorine doped tin oxide (FTO) or indium tin oxide (ITO) substrates, a compact TiO_2 layer, a metal oxide scaffold (such as TiO_2 or Al_2O_3) filled with $CH_3NH_3PbI_3$ or a flat $CH_3NH_3PbI_3$ layer, a hole-transporting material (HTM) layer and a metal back cathode. The HTM layer is inserted between perovskite light-absorbing layer and metal cathode to block electron transfer to the metal back cathode and accelerate the hole transport to the back cathode. Although HTM-free perovskite solar cells have been reported to exhibit impressive cell performance with over 10% efficiency [18, 19], the presence of HTM layers is still advantageous in terms of the inhibition of photogenerated carrier recombination and facilitating the hole transfer, especially for highly efficient solar cells.

Different kinds of HTMs have been developed for perovskite solar cells. Some conjugated polymer HTMs such as polytriarylamine (PTAA), poly-3-hexylthiophene (P3HT), poly[2,5-bis(2-decyldodecyl)(pyrrolo[3,4-c]pyrrole-1,4(2H,5H)-dione-(E)-1,2-di(2,2′-bithiophen-5-yl)ethene] (PDPPDBTE), and poly-[2,1,3-benzothiadiazole-4,7-diyl[4,4-bis(2-ethylhexyl)-4H-cyclopenta[2,1-b:3,4-b′]dithiophene-2,6-diyl]] (PCPDTBT), can exhibit PCEs of over 16% [20–23]. Very recently, inorganic semiconductor HTMs with high hole mobilities (CuI and CuSCN) have also been applied in perovskite solar cells, giving PCEs as high as 12.4%; however, the choice of materials is very limited [24–26]. Typically, special focus has been put on small molecule HTMs due to their definite molecular weights, convenient modification of molecular structures, easy purification and good film-forming properties. Spiro-OMeTAD as a representative small molecule HTM, exhibits extraordinary advantages in this kind of solar cells. PCEs of over 15% have been reported by Grätzel, Snaith and others, in cells based on different mesoporous structures (TiO_2, Al_2O_3) or planar structures [12–15]. However, some disadvantages of spiro-OMeTAD cannot be circumvented, namely the complicated synthetic process and its high price, which are prejudicial to future commercialization. Therefore, seeking appropriate replacements of spiro-OMeTAD with advantages of low-cost, ease of fabrication and high efficiency, is an impending task for scientists.

A few groups have attempted to develop different small molecule HTMs for the perovskite solar cells. For instance, Seok et al. fabricated devices with *N*,*N*-di-p-methoxyphenylamine-substituted pyrene derivatives as HTMs with PCEs of 12.4% [27]. Mhaisalkar et al. used 2,2′,5,5′-tetrakis[*N*,*N*-di(4-methoxyphenyl)amino]-3,3′-bithiophene as HTMs for the device, giving a PCE of 11.4% [28]. Grimsdale et al. reported HTMs based on a triptycene core and electron-rich molecules with 3,4-ethylenedioxythiophene for perovskite solar cells, which exhibited PCEs in the range 12.4%–13.8% [29, 30]. Meng and Li et al. fabricated perovskite solar cells with triphenylamine-based HTMs containing butadiene derivatives with a PCE of 11.63% [31].

In our previous work, we fabricated perovskite solar cells fabricated by a one-step method, using 4,4′-((1E,1′E,3E,3′E)-[1,1′-biphenyl]-4,4′-diylbis(buta-1,3-diene-4,1-diyl))bis(*N*,*N*-di-p-tolylaniline) (2TPA-2-DP) as HTM, which showed a PCE of 9.1% [32]. Here, further optimization of the structure of perovskite solar cells with 2TPA-*n*-DP (n = 1–4) has been carried out, and PCEs as high as 12.96% have been achieved. The interfacial carrier transfer process has been investigated by time-resolved photoluminescence (PL) measurements and electrochemical impedance

spectroscopy (EIS), indicating that 2TPA-*n*-DP has excellent charge transfer and electron blocking ability. Furthermore, the perovskite solar cells with 2TPA-*n*-DP exhibit good stability after storing in a desiccator in the dark for 900 h.

2 Experimental

2.1 Materials

PbI_2 was purchased from Aldrich, *N*,*N*′-dimethylformide (DMF) from Alfar Aesar, hydroiodic acid (AR, 45 wt.% in water) and methylamine (AR, 27% in methanol) from Sinopharm Chemical Reagent Co. Ltd. Spiro-OMeTAD was from Luminescence Technology Corp., Taiwan, China. All the chemicals were directly used without further purification. Methyl ammonium iodide (CH_3NH_3I) was prepared according to the reported procedure [11]. Substrates were FTO conducting glass (Pilkington, thickness: 2.2 mm, sheet resistance: 14 Ω/square). Patterned FTO glass was first cleaned with mild detergent, rinsed several times with distilled water and subsequently with ethanol in an ultrasonic bath, finally dried under air stream.

Four HTMs denoted as 2TPA-*n*-DP (*n* = 1, 2, 3, 4) were obtained according to our previous work [32], and have the structures shown in Scheme 1. The full characterization of 2TPA-*n*-DP (*n* = 2, 3, 4) can be found in the literature [32]. The 2TPA-1-DP was fully characterized by ^{1}H NMR spectrometry, mass spectrometry, IR spectrometry and elemental analysis as follows. ^{1}H NMR (400 MHz, $CDCl_3$) δ (ppm): 7.62 (dd, J = 22.9, 8.4 Hz, 8H), 7.42 (d, J = 8.6 Hz, 4H), 7.20–6.99 (m, 24H), 2.35 (d, J = 23.2 Hz, 12H). IR (cm^{-1}, KBr): 3,031, 2,914, 2,856 (Ar, C–H), 1,596, 1,507 (Ar, C=C), 1,310, 1,281 (C–N), 968 (trans C=C). MS ($APCI^+$), [M^+] 749, calculated value [M] 748. Elemental analysis: calculated for $C_{56}H_{48}N_2$: C, 89.80%; N, 3.74%; H, 6.46%. Found: C, 90.14%; N, 3.73%; H, 6.13%. UV–vis (in CH_2Cl_2): 409, 412 nm.

2.2 Cell fabrication

A 30 nm-thickness compact TiO_2 layer was obtained by spin-coating a mildly acidic solution of titanium isopropoxide in ethanol on the FTO glass, which was subsequently sintered at 500 ℃ for 30 min [30]. Mesoporous TiO_2 films were spin-coated on top of the compact TiO_2 layer using lab-made pastes consisting of 20 nm anatase TiO_2 nanoparticles [33]. Mesoporous TiO_2 layers with thicknesses of 300, 500 and 800 nm were obtained by controlling the TiO_2 contents in the pastes and spin-coating speeds. The TiO_2 scaffolds were sintered at 450 ℃ for 30 min after drying at 80 ℃. Finally, the films were treated in $TiCl_4$ aqueous solution (25 mM) for 40 min at 70 ℃ and sintered at 500 ℃ for 30 min.

The $CH_3NH_3PbI_3$ layer was prepared by a two-step sequential deposition method [15]. First, 1.2 M PbI_2 solution in DMF was spin-coated on TiO_2 mesoporous films at 2,000 rpm for 60 s, then heated at 90 ℃ for 5 min. The films were subsequently immersed into a solution of CH_3NH_3I in isopropanol (10 mg/mL) and the color became dark brown. The films were thoroughly rinsed with isopropanol and finally heated at 90 ℃ for 40 min.

The HTM layers were spin-coated on the top of TiO_2/$CH_3NH_3PbI_3$ films at 3,000 rpm for 20 s. Due to the relatively low solubility of 2TPA-*n*-DP (*n* = 1, 2, 3, 4) in chlorobenzene, slightly different concentrations of the four HTMs were adopted, that is, 2TPA-2-DP (20 mg/mL), 2TPA-1-DP (20 mg/mL), 2TPA-3-DP (15 mg/mL) and 2TPA-4-DP (10 mg/mL), and were kept at 60 ℃ while spin-coating. For comparison, two different perovskite solar cells based on spiro-OMeTAD were also fabricated by using a chlorobenzene solution of undoped material with a concentration of 20 mg/mL (denoted as Sp-A), and a chlorobenzene solution of doped material (denoted as Sp-B) consisting of 83 mg/mL spiro-OMeTAD solution (Sp-B) doped with lithium bis(trifluoromethanesulfonyl)imide (LiTFSI) and 4-tert-butyl pyridine (tBP) [12, 30]. All the above fabrication processes were carried out in air. Finally, a 80 nm-thickness Au photocathode was deposited by thermal evaporation.

2.3 Characterization

Photocurrent–photovoltage characteristics (*J*–*V*) were measured on a Keithley 2602 SourceMeter under AM 1.5 irradiation (100 mW/cm^2) from an Oriel Solar Simulator 91192. A mask with a window of 0.08 cm^2

was clipped on the TiO_2 side to define the photoactive area of the cells. The current–voltage characteristics was scanned at a sweep rate of 0.080 V/s starting from short circuit to forward bias (forward), and back from forward bias to short circuit (backward), and a total of 100 data points were collected with a dwell time of 0.13 s per point. Some hysteresis can also be observed in our device systems (see Fig. S1 in the Electronic Supplementary Material (ESM)), and backward scan curves were adopted here according to the literature [34]. Incident-photon-to-current conversion efficiency (IPCE) was measured by the direct current (DC) method using a lab-made IPCE setup under 0.3–0.9 mW/cm^2 monochromic light illumination without bias illumination [35]. Thickness of films was measured by a surface profiler (KLA-Tencor, P-6). Surface morphologies were characterized by scanning electron microscope (SEM, FEI XL30 S-FEG). Time resolved PL spectra were recorded on PL spectrometer, Edinburgh Instruments, FLS 900, excited with a picosecond pulsed diode laser (EPL-445), and measured at 775 nm after excitation at 445 nm. Electrochemical impedance spectra were obtained at different applied bias under dark conditions on a Zahner IM6e electrochemical workstation in the frequency range from 50 to 10^6 Hz with a perturbation amplitude of 10 mV. The obtained impedance spectra were fitted with Zview software based on an appropriate equivalent circuit. For stability testing, the perovskite solar cells were kept in a desiccator in the dark and tested once a week.

3 Results and discussion

3.1 Molecular structures and energy levels of 2TPA-*n*-DP

The four HTMs 2TPA-*n*-DP (n = 1, 2, 3, 4) were obtained from Horner–Wadsworth–Emmons (HWE) reactions in high yields [32]. It is well known that the glass transition temperature (T_g) has a very important effect on the stability of perovskite solar cells. For the four HTMs, as the number of conjugated ethylene group increases from one to three, the T_g gradually increases from 98, 102 to 164 ℃, and then slightly decreases to 158 ℃ for 2TPA-4-DP. The materials exhibit good thermal stability with decomposition temperatures (T_d) in the range 367–447 ℃. Obviously, their excellent thermal stability can help to stabilize perovskite solar cells.

Scheme 1 presents the molecular structures of the four HTMs and the energy levels of the device. As the number of conjugated ethylene group increases, the HOMO energy levels of 2TPA-*n*-DP gradually increase, and all of them are slightly higher than that of spiro-OMeTAD. Inspiringly, the four HTMs have suitable HOMO levels relative to the valence band of $CH_3NH_3PbI_3$ (–5.43 eV) and Au work function, suggesting that photogenerated carrier dissociation and charge transfer at the interfaces are energetically favorable for $CH_3NH_3PbI_3$ perovskite solar cells. At room temperature, the hole-drift mobilities of 2TPA-*n*-DP (n = 1, 2, 3, 4) are 2.73×10^{-4}, 1.09×10^{-4}, 8.39×10^{-5}

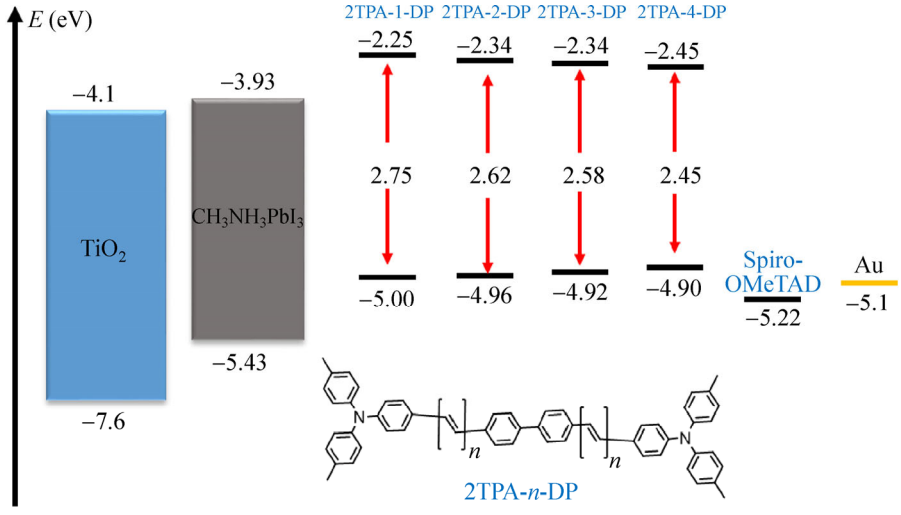

Scheme 1 Chemical structures of 2TPA-*n*-DP (n = 1, 2, 3, 4) and an energy level diagram of perovskite solar cells with 2TPA-*n*-DP.

and 6.79×10^{-5} $cm^2/(V \cdot s)$, respectively, according to time-of-flight (TOF) transient hole-current measurement [32]. The hole mobilities of 2TPA-1-DP and 2TPA-2-DP are quite similar to that of spiro-OMeTAD (2×10^{-4} $cm^2/(V \cdot s)$), whereas those of 2TPA-3-DP and 2TPA-4-DP are slightly lower.

The solubilities in chlorobenzene gradually decrease in the order 2TPA-2-DP > 2TPA-1-DP > 2TPA-3-DP > 2TPA-4-DP, and are all lower than that of spiro-OMeTAD. For example, ~25 mg/mL is the highest solubility of 2TPA-2-DP at room temperature. Therefore, their low solubility cannot give a thick layer in the device.

3.2 Device structure

Figure 1(a) presents the perovskite solar cell configuration and a high-resolution SEM image of the cross-section of the device is given in Fig. 1(b). It can be clearly seen that the device is composed of a 300 nm-thickness FTO substrate, a 30 nm-thickness TiO_2 compact layer, a 500 nm-thickness TiO_2 scaffold with $CH_3NH_3PbI_3$ perovskite, a 200 nm $CH_3NH_3PbI_3$ capping layer, a thin HTM layer and a 80 nm-thickness Au electrode. The perovskite layer was obtained by using a two-step sequential method. According to XRD pattern in Fig. 1(c), the PbI_2 layer was completely converted into $CH_3NH_3PbI_3$, in good agreement with the literature [31]. Good crystallinity of the $CH_3NH_3PbI_3$ layer on TiO_2 film is also observed.

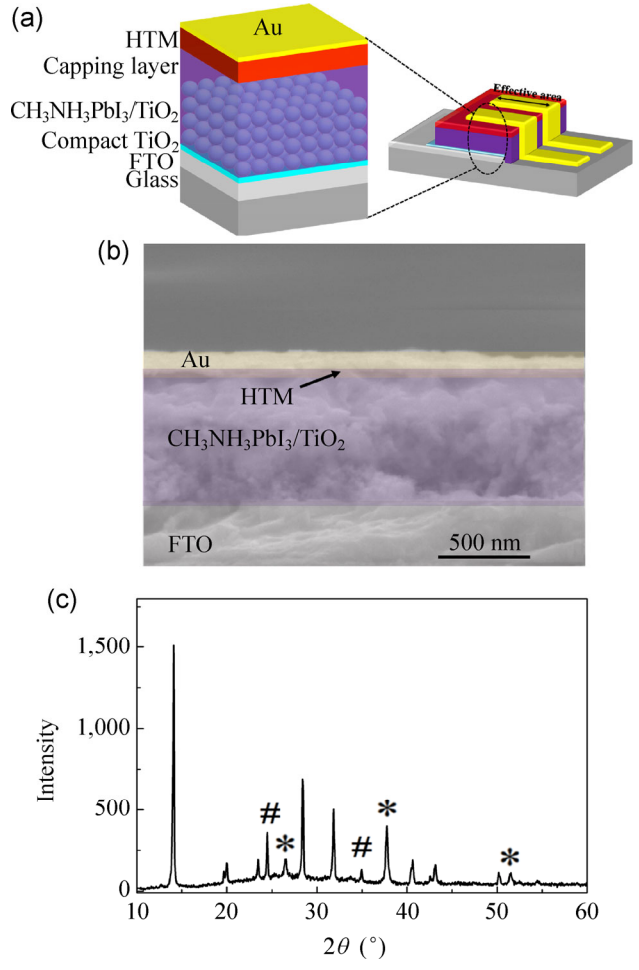

Figure 1 (a) Scheme of the perovskite solar cells based on HTMs; (b) high-resolution cross-sectional SEM image of the $CH_3NH_3PbI_3/TiO_2$/2TPA-n-DP/Au solar cells; (c) XRD pattern (# denotes the peaks of TiO_2 and * the peaks of FTO).

3.3 Photocurrent density–photovoltage (*J–V*) characteristics

First, effect of the TiO_2 film thickness on the cell performance was investigated, using $CH_3NH_3PbI_3$ perovskite solar cells with 2TPA-2-DP. Figure 2 presents the photocurrent density–photovoltage characteristics of the devices and detailed photovoltaic parameters are given in Table 1. The short-circuit current density (J_{sc}) increases from 14.73 to 19.33 mA/cm^2 when the film thickness increases from 300 to 500 nm since greater $CH_3NH_3PbI_3$ deposition can result in more photogenerated electrons. However, when the film thickness further increases to 800 nm, recombination becomes too fast, leading to lower J_{sc} (17.70 mA/cm^2) and poor PCEs [11, 36]. With increasing TiO_2 film thickness, the open circuit voltage (V_{oc}) gradually decreases from 973.7, 942.2 to 910.7 mV, mainly due to the faster recombination. Therefore, 500 nm-thickness

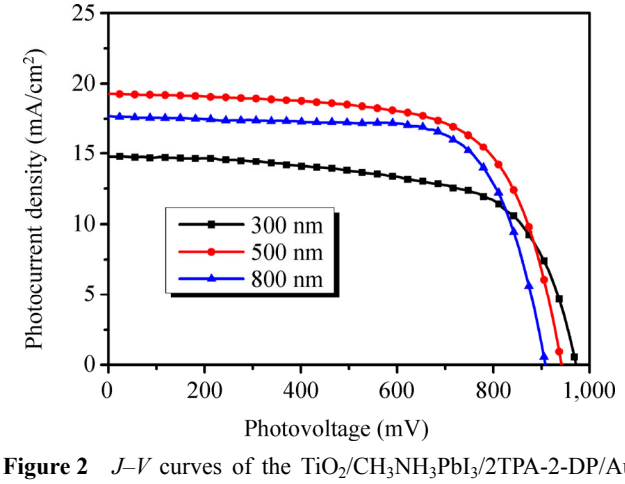

Figure 2 *J–V* curves of the $TiO_2/CH_3NH_3PbI_3$/2TPA-2-DP/Au solar cells with different TiO_2 film thicknesses.

Table 1 Effect of TiO_2 thickness on cell performance of the devices with 2TPA-2-DP under AM 1.5 illumination (100 mW/cm^2)

Thickness (nm)	J_{sc} (mA/cm^2)	V_{oc} (mV)	FF	PCE (%)
300	14.73	973.7	0.652	9.35
500	19.33	942.2	0.674	12.29
800	17.70	910.7	0.713	11.49

TiO_2 scaffold is the best choice for our $CH_3NH_3PbI_3$ perovskite solar cells with 2TPA-2-DP, and is adopted in the following investigation.

Based on a 500 nm-thickness TiO_2 scaffold, a series of $CH_3NH_3PbI_3$ perovskite solar cells with 2TPA-*n*-DP (*n* = 1, 2, 3, 4) as HTMs were fabricated, as shown in Fig. 3(a) and Table 2. For the three devices based on 2TPA-*n*-DP (*n* = 1, 2, 3), there is no obvious difference in J_{sc}, suggesting a small difference in the charge collection of the HTMs. In addition, no obvious variation was found in V_{oc} of these devices which is consistent with there being no significant difference in the HOMO levels for the three 2TPA-*n*-DP (*n* = 1, 2, 3). PCEs of over 12% are obtained for the devices with 2TPA-1-DP, 2TPA-2-DP and 2TPA-3-DP. However, the cell performance of the device with 2TPA-4-DP is relatively poor, with low values of J_{sc} and V_{oc} [37]. As we mentioned in the Experimental section, the concentration of 2TPA-4-DP in chlorobenzene is only 10 mg/mL, much lower than for other HTMs. According to our recent investigation, low volume ratios of the HTM in the device will result in insufficient pore-filling fraction and incomplete coverage on the surface of $CH_3NH_3PbI_3$, thus leading to the rapid recombination between the photogenerated electrons and holes on the Au electrode, which is in good agreement with the decrease in J_{sc}, V_{oc} and PCE of the device with 2TPA-4-DP [38]. Obviously, the unsatisfactory solubility of 2TPA-4-DP has a negative influence on the performance of the cell, whereas PCEs as high as 12.96% were obtained for the device based on 2TPA-2-DP. Therefore, further investigation on the interfacial charge transfer process of the devices employed perovskite solar cells with 2TPA-2-DP, is described in the following discussion.

For comparison, perovskite solar cells without

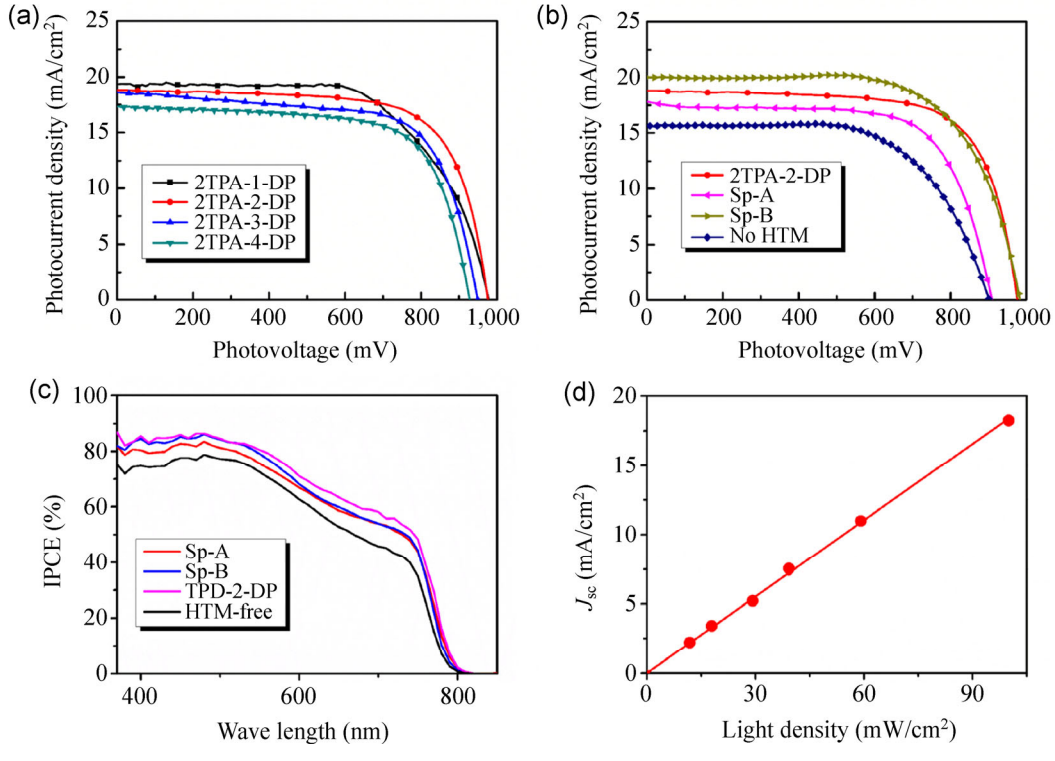

Figure 3 (a) *J*–*V* curves of a series of $TiO_2/CH_3NH_3PbI_3$/ HTM/Au solar cells (HTMs = 2TPA-*n*-DP (*n* = 1, 2, 3, 4)), (b) *J*–*V* curves and (c) IPCE spectra of $TiO_2/CH_3NH_3PbI_3$/HTM/Au solar cells (HTMs = 2TPA-2-DP, Sp-A and Sp-B) and the $CH_3NH_3PbI_3/TiO_2$/Au solar cell; (d) the relationship of the J_{sc} of the 2TPA-2-DP-based device with different light densities.

HTMs (TiO_2/$CH_3NH_3PbI_3$/Au) were also fabricated, and had values of J_{sc}, V_{oc} and FF of 15.70 mA/cm², 900.8 mV and 0.638, respectively, yielding an overall PCE of 9.03% [19], as shown in Fig. 3(b). When HTMs are introduced into the devices, the cell performance significantly improves under the same conditions, especially in terms of the values of J_{sc}, V_{oc} and PCE, as illustrated in Table 2. Obviously, the presence of HTMs is advantageous in terms of inhibiting electron transfer from $CH_3NH_3PbI_3$ to the Au electrode and facilitating the hole transport to Au electrode. The cell performances of the devices with conventional spiro-OMeTAD are also given. As we can see from Fig. 3(b) and Table 2, the device with Sp-A (the same concentration as the 2TPA-2-DP) shows a PCE of 11.46% with J_{sc} of 18.25 mA/cm², V_{oc} of 910.7 mV and FF of 0.690, values which are lower than those of the devices with 2TPA-*n*-DP (*n* = 1, 2, 3). When the perovskite solar cells with Sp-A and Sp-B are compared, it is found that the doped spiro-OMeTAD (Sp-B) can give better conductivity than the undoped one (Sp-A), leading to better J_{sc}, V_{oc} and PCEs (13.22% vs. 11.46%), in good agreement with the literature [27]. Unfortunately, doping 2TPA-*n*-DP (*n* = 1, 2, 3, 4) with LiTFSI and tBP in a similar fashion, did not show encouraging results. Further attempts will be carried out in the future.

Table 2 Parameters of photovoltaic performance of the devices with different HTMs under AM 1.5 illumination (100 mW/cm²)

HTMs	J_{sc} (mA/cm²)	V_{oc} (mV)	FF	PCE (%)
2TPA-1-DP	19.16	973.7	0.662	12.34
2TPA-2-DP	18.82	973.7	0.707	12.96
2TPA-3-DP	18.67	951.5	0.688	12.22
2TPA-4-DP	17.30	928.6	0.696	11.18
Sp-A	18.25	910.7	0.690	11.46
Sp-B	20.08	980.3	0.670	13.22
HTM-free	15.70	900.8	0.638	9.03

The monochromatic IPCE spectra of the devices with 2TPA-2-DP, Sp-A and Sp-B and the HTM-free device are presented in Fig. 3(c). Integral photocurrents from the overlap of the IPCE spectra are 17.7, 16.7, 17.0 and 15.2 mA/cm² for the devices with 2TPA-2-DP, Sp-A and Sp-B and the HTM-free device, respectively, in good agreement with the experimental values of J_{sc} [31].

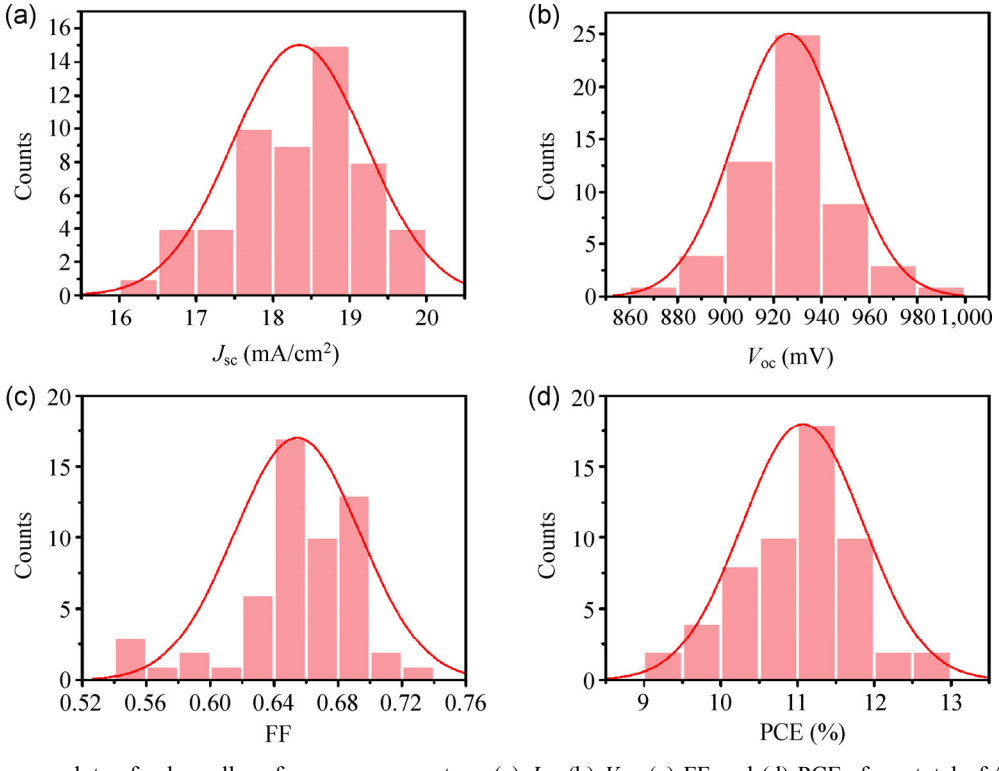

Figure 4 Histogram plots of solar cell performance parameters: (a) J_{sc}; (b) V_{oc}; (c) FF and (d) PCEs for a total of 56 samples with 2TPA-2-DP as the HTM. The normal fitting has been added to aid the eye.

Furthermore, the relationship between the J_{sc} of the solar cell with 2TPA-2-DP and different light intensities is investigated, as shown in Fig. 3(d). Good linearity is observed, indicating that the hole collection ability of 2TPA-2-DP in the perovskite solar cell is independent of light density. According to previous investigations, it is believed that there is no obvious space–charge limit in the $TiO_2/CH_3NH_3PbI_3$/2TPA-2-DP junction due to small difference in the mobility between electrons and holes [11, 31, 39].

As a preliminary investigation of the reproducibility of our devices, 56 different solar cells with 2TPA-2-DP were prepared under the same conditions. As shown in Fig. 4, the samples have average values of J_{sc}, V_{oc}, FF and PCE of 18.3 ± 0.97 mA/cm², 926.4 ± 22.4 mV, 0.65 ± 0.04 and 11.06% ± 0.79%, respectively. A total of 18 samples gave PCEs between 11.0% and 11.5%. This suggests that the reproducibility of our perovskite solar cells is fairly good [15].

3.4 Photoluminescence measurements

In order to further understand the charge separation and collection processes in $CH_3NH_3PbI_3$ perovskite solar cells with HTMs, time-resolved PL decay measurements of three samples—$TiO_2/CH_3NH_3PbI_3$, $TiO_2/CH_3NH_3PbI_3$/2TPA-2-DP and $TiO_2/CH_3NH_3PbI_3$/spiro-OMeTAD films were carried out [40]. Among the three samples, the $TiO_2/CH_3NH_3PbI_3$ film exhibits the longest PL decay time, whereas the TiO_2/perovskite/2TPA-2-DP film has shortest PL lifetime, as shown in Fig. 5. The PL decay times of three samples, which are obtained by fitting the data with a bi-exponential decay function, are presented in Table 3.

For the $TiO_2/CH_3NH_3PbI_3$ film without a HTM layer, the PL lifetime is 103.73 ns. When coated with a thin HTM layer on the surface of $CH_3NH_3PbI_3$, the PL lifetime significantly decreases to 19.9 ns for the $TiO_2/CH_3NH_3PbI_3$/Sp-B film and 8.52 ns for $TiO_2/CH_3NH_3PbI_3$/2TPA-2-DP film. The shortening of the PL lifetime can be attributed to the HTM layer quenching photogenerated excitons at the perovskite/HTM interface [40, 41]. It is thus suggested that the existence of $CH_3NH_3PbI_3$/HTM interface enhances the hole transfer. In addition, based on the same $TiO_2/CH_3NH_3PbI_3$ film, the quenching ability of 2TPA-2-DP is stronger than that of Sp-B, which indicates the excellent charge

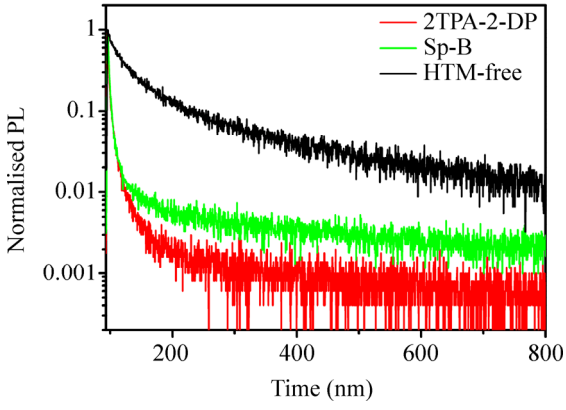

Figure 5 Time-resolved PL spectra of $TiO_2/CH_3NH_3PbI_3$, $TiO_2/CH_3NH_3PbI_3$/2TPA-2-DP and $TiO_2/CH_3NH_3PbI_3$/Sp-B films, monitored at 775 nm during the transformation. Excitation wavelength: 445 nm.

Table 3 PL lifetimes of $TiO_2/CH_3NH_3PbI_3$, $TiO_2/CH_3NH_3PbI_3$/2TPA-2DP and $TiO_2/CH_3NH_3PbI_3$/Sp-B films

HTM	*T*1 (ns)	*T*2 (ns)
HTM-free	103.73	16.21
2TPA-2-DP	8.52	1.33
Sp-B	19.9	2.09

transfer ability of 2TPA-2-DP [42, 43]. Accordingly, the HTM-free perovskite solar cells have poor PCE values in comparison to the other two HTM-based devices. However, the device with Sp-B exhibits better cell performance than that with 2TPA-2-DP, although this is inconsistent with their respective PL lifetimes. This is mainly due to the Sp-B layer (~200 nm) being thicker than 2TPA-2-DP (no visible overlayer) and thus being able to restrain the photogenerated carrier recombination on the Au electrode.

3.5 Electrochemical impedance spectra

EIS is generally considered a very useful tool to investigate internal electrical processes of solar cells, and helps us to analyze the interfacial electron transfer and recombination processes [24, 44, 45]. In solid-state perovskite solar cells with a mesoporous TiO_2 scaffold, several interfaces are involved, such as FTO/compact TiO_2 layer/mesoporous TiO_2 layer, TiO_2 layer/perovskite, perovskite/HTM and HTM/Au, and these can be well described by the full model proposed by Grätzel et al. [44]. Depending on the EIS measurement conditions (in the dark or under irradiation, high or low forward

bias) and fabrication techniques, some interfacial effects need to be emphasized, whereas others can be neglected [44].

Here, EIS is employed to understand the electron blocking ability of HTMs in our perovskite solar cells. Nyquist plots of three devices with Sp-A, Sp-B, 2TPA-2-DP as HTMs and the HTM-free device with a potential bias of 600 mV in the dark in the frequency range from 10^6 to 50 Hz, are given in Fig. 6(a). We can see that, two RC (a resistance (R) in parallel with a capacity (C)) arcs are observed in three devices with Sp-A, Sp-B and 2TPA-2-DP, whereas no obvious high frequency arc is observed for the HTM-free device. Generally, a high frequency arc is associated with the back contact at the Au/HTM interface (see the inset of Fig. 6(a)), which can be expressed as a constant phase element (CPE2) of HTMs for better fitting. At lower frequency response, the arc is related to charge transfer at the TiO_2/perovskite/HTM interfaces, mainly due to the recombination of electrons from the mesoporous TiO_2 with holes in the HTM. These might have to go through the perovskite layer in our device system with the sub-micrometer mesoporous TiO_2 layer mostly covered by perovskite and subsequently with the HTM [45].

The above plots were fitted by Zview software and using the equivalent circuit shown in Fig. 6(b), which is derived from the transmission line model [24, 44, 45]. R_{ct}, which is defined as the charge transfer resistance at TiO_2/perovskite/HTM interfaces, is related to the electron blocking ability of HTM. Better electron blocking ability of the HTM can prevent electron transport from TiO_2/perovskite to HTM, thus resulting in larger R_{ct}. R_{ct} is obtained by fitting the Nyquist plots at different bias potentials, as shown in Fig. 6(c). For the device with the 2TPA-2-DP layer, at low potential bias (100–500 mV), small changes in R_{ct} are found, whereas the value of R_{ct} decreases markedly with increasing bias potential in the range 500 to 1,000 mV. This is mainly due to the Fermi level of the mesoscopic TiO_2 being elevated under forward bias (>500 mV), which enhances electron flow across the TiO_2/$CH_3NH_3PbI_3$ interface. For the same forward bias voltage, the values of R_{ct} of three HTM layers (Sp-A, Sp-B and 2TPA-2-DP) are quite similar, indicating that 2TPA-2-DP can also act as an excellent electron blocking layer similar to spiro-OMeTAD.

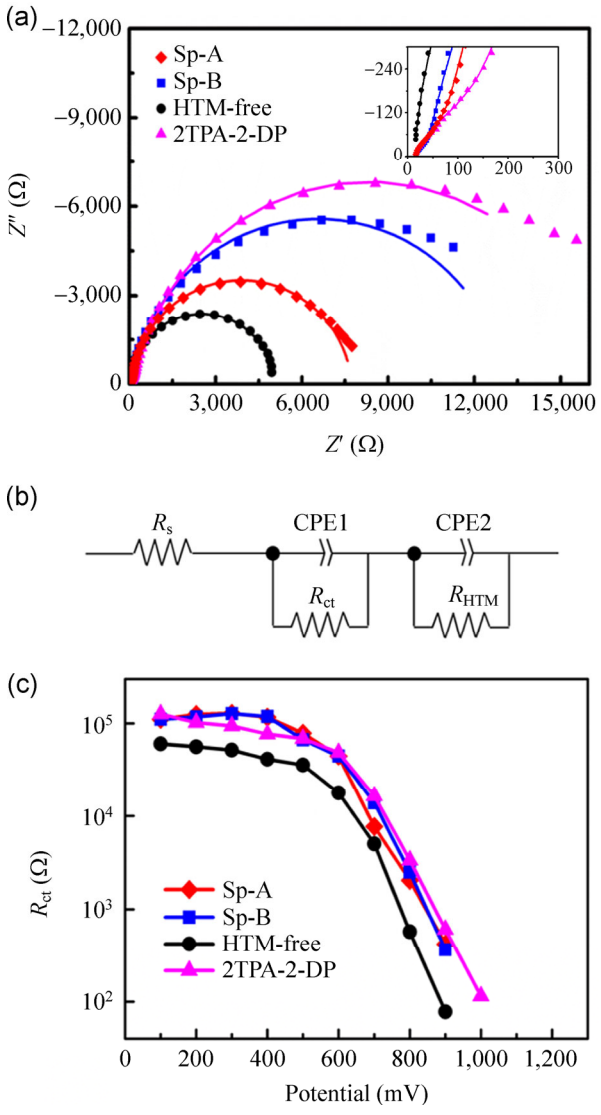

Figure 6 (a) Nyquist plots of the devices with 2TPA-2-DP, Sp-A, Sp-B and HTM-free layer measured at a bias potential of 600 mV in dark conditions. Inset: The abscissa expanded in the high frequency range. The scattered points are experimental data and the solid lines are the fitting curves. (b) Equivalent circuit for fitting curves, R_s: series resistance; R_{ct}: charge transfer resistance at the TiO_2/$CH_3NH_3PbI_3$/HTM interfaces; CPE: constant phase element of electrical double layer. (c) Dependence of fitted charge transfer resistance (R_{rec}) on different bias potentials.

3.6 Stability tests

Long term stability of the components of the device and the device itself are important parameters for solar cells. A preliminary stability test of perovskite solar cells with 2TPA-*n*-DP (*n* = 1, 2, 3, 4) was carried out by storing the unsealed devices in a desiccator at room temperature for 900 h and testing them once every

4–5 days. As shown in Fig. 7, the PCEs of the four devices increase slightly in the first 200 h, since the values of J_{sc} slightly improved while the other parameters remained constant. During the whole conservation time, parameters for devices with 2TPA-*n*-DP (*n* = 1, 2, 3) retained over 90% of their initial values, with the values of J_{sc} and FF slightly decreasing and V_{oc} remaining almost constant, indicating they have promising long-term stability at room temperature.

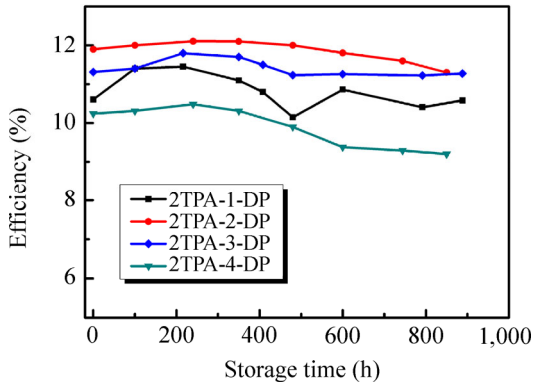

Figure 7 Efficiencies of perovskite solar cells with 2TPA-*n*-DP (*n* = 1, 2, 3, 4) versus storage time.

4 Conclusions

$CH_3NH_3PbI_3$ perovskite solar cells with 2TPA-*n*-DP (*n* = 1, 2, 3, 4) hole-transporting layers have been successfully fabricated. By adopting a two-step sequential perovskite deposition method and optimization of TiO_2 film thickness, PCE values of up to 12.96% have been achieved for the device with 2TPA-2-DP. The charge separation and collection processes have been studied by photoluminescence measurements. The PL quenching time decreases from 103.73 to 8.52 ns after the 2TPA-2-DP is introduced into the TiO_2/$CH_3NH_3PbI_3$ film, indicating that the HTM layer can effectively quench photogenerated excitons at the perovskite/HTM interface. Further investigation by EIS reveals that the charge transfer resistance of the HTM-based devices is higher than for the HTM-free case, indicating the good electron blocking ability of 2TPA-*n*-DP. Indeed, 2TPA-2-DP exhibits an electron blocking ability comparable to that of spiro-OMeTAD. Therefore, it is suggested that the 2TPA-*n*-DP hole-transporting films may be promising alternatives to conventional spiro-OMeTAD films. Furthermore, the solar cells with a thin 2TPA-*n*-DP hole-transporting layer show good stability when kept at room temperature for 900 h.

Acknowledgements

The authors would like to thank the following for financial support: The National Basic Research Program of China (Nos. 2012CB932903 and 2012CB932904), Beijing Science and Technology Committee (No. Z131100006013003), the National Natural Science Foundation of China (Nos. 51372272, 11474333, 9123302, 51372270 and 21173260) and the Knowledge Innovation Program of the Chinese Academy of Sciences.

Electronic Supplementary Material: Supplementary materials (further details of the full *J*–*V* curve (both forward and backward)) is available in the online version of this article at http://dx.doi.org/10.1007/s12274-014-0592-y.

References

[1] Baikie, T.; Fang, Y. N.; Kadro, J. M.; Schreyer, M.; Wei, F. X.; Mhaisalkar, S. G.; Grätzel, M.; White, T. J. Synthesis and crystal chemistry of the hybrid perovskite $(CH_3NH_3)PbI_3$ for solid-state sensitised solar cell applications. *J. Mater. Chem. A* **2013**, *1*, 5628–5641.

[2] Feng, J.; Xiao, B. Crystal structures, optical properties, and effective mass tensors of $CH_3NH_3PbX_3$ (*X* = I and Br) phases predicted from HSE06. *J. Phys. Chem. Lett.* **2014**, *5*, 1278–1282.

[3] Kazim, S.; Nazeeruddin, M. K.; Grätzel, M.; Ahmad, S. Perovskite as light harvester: A game changer in photovoltaics. *Angew. Chem. Int. Ed.* **2014**, *53*, 2812–2824.

[4] Stoumpos, C. C.; Malliakas, C. D.; Kanatzidis, M. G. Semiconducting tin and lead iodide perovskites with organic cations: Phase transitions, high mobilities, and near-infrared photoluminescent properties. *Inorg. Chem.* **2013**, *52*, 9019–9038.

[5] Ponseca, C. S. Jr.; Savenije, T. J.; Abdellah, M.; Zheng, K. B.; Yartsev, A.; Pascher, T.; Harlang, T.; Chabera, P.; Pullerits, T.; Stepanov, A. et al. Organometal halide perovskite solar cell materials rationalized: Ultrafast charge generation, high and microsecond-long balanced mobilities, and slow recombination. *J. Am. Chem. Soc.* **2014**, *136*, 5189–5192.

[6] Snaith, H. J. Perovskites: The emergence of a new era for low-cost, high-efficiency solar cells. *J. Phys. Chem. Lett.* **2013**, *4*, 3623–3630.

[7] Park, N.G. Organometal perovskite light absorbers toward a 20% efficiency low-cost solid-state mesoscopic solar cell. *J. Phys. Chem. Lett.* **2013**, *4*, 2423–2429.

[8] Bretschneider, S. A.; Weickert, J.; Dorman, J. A.; Schmidt-Mende, L. Research update: Physical and electrical characteristics of lead halide perovskites for solar cell applications. *APL Mater*. **2014**, *2*, 040701.

[9] Kojima, A.; Teshima, K.; Shirai, Y.; Miyasaka, T. Organometal halide perovskites as visible-light sensitizers for photovoltaic cells. *J. Am. Chem. Soc.* **2009**, *131*, 6050–6051.

[10] Li, W. Z.; Li, J. L.; Wang, L. D.; Niu, G. D.; Gao, R.; Qiu, Y. Post modification of perovskite sensitized solar cells by aluminum oxide for enhanced performance. *J. Mater. Chem. A* **2013**, *1*, 11735–11740.

[11] Kim, H. S.; Lee, C. R.; Im, J. H.; Lee, K. B.; Moehl, T.; Marchioro, A.; Moon, S. J.; Humphry-Baker, R.; Yum, J. H.; Moser, J. E. et al. Lead iodide perovskite sensitized all-solid-state submicron thin film mesoscopic solar cell with efficiency exceeding 9%. *Sci. Rep.* **2012**, *2*, 591.

[12] Liu, M. Z.; Johnston, M. B.; Snaith, H. J. Efficient planar heterojunction perovskite solar cells by vapour deposition. *Nature* **2013**, *501*, 395–402.

[13] Xiao, Z. G.; Bi, C.; Shao, Y. C.; Dong, Q. F.; Wang, Q.; Yuan, Y. B.; Wang, C. G.; Gao, Y. L.; Huang, J. S. Efficient, high yield perovskite photovoltaic devices grown by interdiffusion of solution-processed precursor stacking layers. *Energy Environ. Sci.* **2014**, *7*, 2619–2623.

[14] Liu, D. Y.; Kelly, T. L. Perovskite solar cells with a planar heterojunction structure prepared using room-temperature solution processing techniques. *Nat. Photonics* **2014**, *8*, 133–138.

[15] Burschka, J.; Pellet, N.; Moon, S. J.; Humphry-Baker, R.; Gao, P.; Nazeeruddin, M. K.; Grätzel M. Sequential deposition as a route to high-performance perovskite-sensitized solar cells. *Nature* **2013**, *499*, 316–320.

[16] NREL. *Best Research-Cell Efficiencies* [Online]. http://www.nrel.gov/ncpv/images/efficiency_chart.jpg (accessed June 30, 2014).

[17] Service, R. F. Energy technology perovskite solar cells keep on surging. *Science* **2014**, *344*, 458–458.

[18] Laban, W. A.; Etgar, L. Depleted hole conductor-free lead halide iodide heterojunction solar cells. *Energy Environ. Sci.* **2013**, *6*, 3249–3253.

[19] Shi, J. J.; Dong, J.; Lv, S. T.; Xu, Y. Z.; Zhu, L. F.; Xiao, J. Y.; Xu, X.; Wu, H. J.; Li, D. M.; Luo, Y. H. et al. Hole-conductor-free perovskite organic lead iodide heterojunction thin-film solar cells: High efficiency and junction property. *Appl. Phys. Lett.* **2014**, *104*, 063901.

[20] Kwon, Y. S.; Lim, J.; Yun, H. J.; Kim, Y. H.; Park, T. A diketopyrrolopyrrole-containing hole transporting conjugated polymer for use in efficient stable organic-inorganic hybrid solar cells based on a perovskite. *Energy Environ. Sci.* **2014**, *7*, 1454–1460.

[21] Heo, J. H.; Im, S. H.; Noh, J. H.; Mandal, T. N.; Lim, C. S.; Chang, J. A.; Lee, Y. H.; Kim, H. J.; Sarkar, A.; Nazeeruddin, M. K. et al. Efficient inorganic-organic hybrid heterojunction solar cells containing perovskite compound and polymeric hole conductors. *Nat. Photonics* **2013**, *7*, 486–491.

[22] Di Giacomo, F.; Razza, S.; Matteocci, F.; D'Epifanio, A.; Licoccia, S.; Brown, T. M.; Di Carlo, A. High efficiency $CH_3NH_3PbI_{(3-x)}Cl_{1-x}$ perovskite solar cells with poly(3-hexylthiophene) hole transport layer. *J. Power Sources* **2014**, *251*, 152–156.

[23] Ryu, S. C.; Noh, J. H.; Jeon, N. J.; Kim, Y. C.; Yang, W. S.; Seo, J. W.; Seok, S. I. Voltage output of efficient perovskite solar cells with high open-circuit voltage and fill factor. *Energy Environ. Sci.* **2014**, *7*, 2614–2618.

[24] Christians, J. A.; Fung, R. C. M.; Kamat, P. V. An inorganic hole conductor for organo-lead halide perovskite solar cells. Improved hole conductivity with copper iodide. *J. Am. Chem. Soc.* **2014**, *136*, 758–764.

[25] Ito, S.; Tanaka, S.; Vahlman, H.; Nishino, H.; Manabe, K.; Lund, P. Carbon-double-bond-free printed solar cells from $TiO_2/CH_3NH_3PbI_3$/CuSCN/Au: Structural control and photoaging effects. *ChemPhysChem* **2014**, *15*, 1194–1200.

[26] Qin, P.; Tanaka, S.; Ito, S.; Tetreault, N.; Manabe, K.; Nishino, H.; Nazeeruddin, M. K.; Grätzel, M. Inorganic hole conductor-based lead halide perovskite solar cells with 12.4% conversion efficiency. *Nat. Commun.* **2014**, *5*, 3834.

[27] Jeon, N. J.; Lee, J.; Noh, J. H.; Nazeeruddin, M. K.; Graetzel, M.; Seok, S. I. Efficient inorganic organic hybrid perovskite solar cells based on pyrene arylamine derivatives as hole-transporting materials. *J. Am. Chem. Soc.* **2013**, *135*, 19087–19090.

[28] Krishnamoorthy, T.; Fu, K. W.; Boix, P. P.; Li, H. R.; Koh, T. M.; Leong, W. L.; Powar, S.; Grimsdale, A.; Grätzel, M.; Mathews, N. et al. A swivel-cruciform thiophene based hole-transporting material for efficient perovskite solar cells. *J. Mater. Chem. A* **2014**, *2*, 6305–6309.

[29] Li, H. R.; Fu, K. W.; Hagfeldt, A.; Grätzel, M.; Mhaisalkar, S. G.; Grimsdale, A. C. A simple 3,4-ethylenedioxythiophene based hole-transporting material for perovskite solar cells. *Angew. Chem. Int. Ed.* **2014**, *53*, 4085–4088.

[30] Krishna, A.; Sabba, D.; Li, H. R.; Yin, J.; Boix, P. P.; Soci, C.; Mhaisalkar, S. G.; Grimsdale, A. C. Novel hole

transporting materials based on triptycene core for high efficiency mesoscopic perovskite solar cells. *Chem. Sci.* **2014**, *5*, 2702–2709.

[31] Lv, S. T.; Han, L. Y.; Xiao, J. Y.; Zhu, L. F.; Shi, J. J.; Wei, H. Y.; Xu, Y. Z.; Dong, J.; Xu, X.; Li, D. M. et al. Mesoscopic $TiO_2/CH_3NH_3PbI_3$ perovskite solar cells with new hole-transporting materials containing butadiene derivatives. *Chem. Commun.* **2014**, *50*, 6931–6934.

[32] Wang, J. J.; Wang, S. R.; Li, X. G.; Zhu, L. F.; Meng, Q. B.; Xiao, Y.; Li, D. M. Novel hole transporting materials with a linear pi-conjugated structure for highly efficient perovskite solar cells. *Chem. Commun.* **2014**, *50*, 5829–5832.

[33] Ito, S.; Murakami, T. N.; Comte, P.; Liska, P.; Grätzel, C.; Nazeeruddin, M. K.; Grätzel, M. Fabrication of thin film dye sensitized solar cells with solar to electric power conversion efficiency over 10%. *Thin Solid Films* **2008**, *516*, 4613–4619.

[34] Snaith, H. J.; Abate, A.; Ball, J. M.; Eperon, G. E.; Leijtens, T.; Noel, N. K.; Stranks, S. D.; Wang, J. T.W.; Wojciechowski, K.; Zhang, W. Anomalous hysteresis in perovskite solar cells. *J. Phys. Chem. Lett.* **2014**, *5*, 1511–1515.

[35] Guo, X. Z.; Luo, Y. H.; Zhang Y. D.; Huang, X. C.; Li, D. M.; Meng, Q. B. Study on the effect of measuring methods on incident photon-to-electron conversion efficiency of dye-sensitized solar cells by home-made setup. *Rev. Sci. Instrum.* **2010**, *81*, 103106.

[36] Zhao, Y. X.; Zhu, K. Charge transport and recombination in perovskite $CH_3NH_3PbI_3$ sensitized TiO_2 solar cells. *J. Phys. Chem. Lett.* **2013**, *4*, 2880–2884.

[37] Xu, Y. Z.; Shi, J. J.; Lv, S. T.; Zhu, L. F.; Dong, J.; Wu, H. J.; Xiao, Y.; Luo, Y. H.; Wang, S. R.; Li, D. M. et al. Simple way to engineer metal-semiconductor interface for enhanced performance of perovskite organic lead iodide solar cells. *ACS Appl. Mater. Interfaces* **2014**, *6*, 5651–5656.

[38] Xiao, J. Y.; Han, L. Y.; Zhu, L. F.; Lv, S. T.; Shi, J. J.; Wei, H. Y.; Xu, Y. Z.; Dong, J.; Xu, X.; Xiao, Y. et al. A thin pristine non-triarylamine hole-transporting material layer for efficient $CH_3NH_3PbI_3$ perovskite solar cells. *RSC Adv.* **2014**, *4*, 32918–32923.

[39] Koster, L. J. A.; Mihailetchi, V. D.; Xie, H.; Blom, P. W. M. Origin of the light intensity dependence of the short-circuit current of polymer/fullerence solar cells. *Appl. Phys. Lett.* **2005**, *87*, 203502.

[40] You, J. B.; Hong, Z. R.; Yang, Y.; Chen, Q.; Cai, M.; Song, T.B.; Chen, C.C.; Lu, S. R.; Liu, Y. S.; Zhou, H. P. Low-temperature solution-processed perovskite solar cells with high efficiency and flexibility. *ACS Nano* **2014**, *8*, 1674–1680.

[41] Xing, G. C.; Mathews, N.; Sun, S. Y.; Lim, S. S.; Lam, Y. M.; Grätzel, M.; Mhaisalkar, S.; Sum, T. C. Long-range balanced electron- and hole-transport lengths in organic-inorganic $CH_3NH_3PbI_3$. *Science* **2013**, *342*, 344–347.

[42] Stranks, S. D.; Eperon, G. E.; Grancini, G.; Menelaou, C.; Alcocer, M. J. P.; Leijtens, T.; Herz, L. M.; Petrozza, A.; Snaith, H. J. Electron-hole diffusion lengths exceeding 1 micrometer in an organometal trihalide perovskite absorber. *Science* **2013**, *342*, 341–344.

[43] Shaw, P. E.; Ruseckas, A.; Samuel, I. D. W. Exciton diffusion measurements in poly(3-hexylthiophene). *Adv. Mater.* **2008**, *20,* 3516–3520.

[44] Dualeh, A.; Moehl, T.; Tetreault, N.; Teuscher, J.; Gao, P.; Nazeeruddin, M. K.; Grätzel, M. Impedance spectroscopic analysis of lead iodide perovskite-sensitized solid-state solar cells. *ACS Nano* **2014**, *8*, 362–373.

[45] Kim, H. S.; Mora-Sero, I.; Gonzalez-Pedro, V.; Fabregat-Santiago, F.; Juarez-Perez, E. J.; Park, N. G.; Bisquert, J. Mechanism of carrier accumulation in perovskite thin-absorber solar cells. *Nat. Commun.* **2013**, *4*, 2242.